Conference Paper, Published Version

Barranco, Ignacio; Higuera, Pablo; Liu, Philip L.-F.

Physical and Numerical Modelling of Tsunami-Like Bores Surf and Swash Flows

Coastal Structures 2019 - Nils Goseberg, Torsten Schlurmann (eds) - © 2019 Bundesanstalt für Wasserbau
ISBN 978-3-939230-64-9 (Online) - DOI: 10.18451/978-3-939230-64-9_055

Physical and Numerical Modelling of Tsunami-Like Bores Surf and Swash Flows

I. Barranco[1], P. Higuera[1] & P. L.-F. Liu[1,2,3]
[1]*Department of Civil and Environmental Engineering, National University of Singapore, Singapore*
[2]*School of Civil and Environmental Engineering, Cornell University, USA*
[3]*Institute of Hydrological and Oceanic Sciences, National Central University, Taiwan*

Abstract: Tsunamis are very large transient sea waves usually produced by submarine earthquakes or landslides. When these waves reach coastal areas, they can cause severe damage and losses. The aim of this study is to extend the knowledge on tsunami inundation processes by reproducing realistic physical and numerical tsunami surf and swash flows. The experimental results presented in this work point out the important role the waves period play in the flooding processes. In addition, these results have been used to further validate the numerical model employed.

Keywords: Tsunami, coastal flooding, bore, physical modelling, run-up, PIV, CFD

1 Introduction

Understanding the impact and flooding processes of tsunamis is essential to assess tsunami hazard and risk analysis. To understand better these processes, scientists have simulated tsunami-like waves reaching coastal areas both physically and numerically.

Tsunamis have been generated in laboratories using different generation systems. Two commonly used systems are: 1) Piston-type wavemakers have been designed to generate specific wave forms such as solitary waves (e.g. Liu et al. 1995; Synolakis 1987) and elongated solitons (Schimmels et al. 2016); 2) Dam-break systems suddenly release a stored volume of water to generate bore waves (e.g. Imamura et al. 2008). Other mechanisms have also been employed to simulate tsunamis by controlling the flumes' water in-flows (Rossetto et al. 2011, Goseberg et al. 2013).

However, due to the large length of these waves, the scale of some of these experiments is too large to study in detail the generated swash flows, or, alternatively, the generated wave lengths are too short to simulate the whole flooding processes.

The aim of this study is to reproduce physically realistic tsunami surf and swash flows to understand better the impact of tsunamis on the coast. Due to the scale differences between the offshore processes (i.e. tsunami generation and propagation) and the coastal processes (i.e. wave breaking, inundation, impact and sediment transport), and because of the laboratory physical limitations, this study focuses on the generation of realistic tsunami fronts reaching coastal areas. To reproduce these tsunami fronts, a long piston wavemaker (WM hereinafter) and a large reservoir dam-break system (DB hereinafter) are used. Finally, the propagation of these waves over a constant water depth flume and the generated swash flows over a glass slope are analyzed, including run-up and inundation depths. The experimental results, including flow velocity measurements, are then compared with numerical results for validation purposes.

2 Tsunamis in coastal areas

To simulate realistic tsunami waves, careful observations from past events have to be taken. The 2004 Indian Ocean tsunami reached the coast of Thailand in the form of long breaking undulating bores and flooded coastal areas for periods of minutes. During the 2011 Japan tsunami, the first tsunami wave

was the largest wave observed in the Miyagi Prefecture, but in other areas subsequent waves were larger (Mori et al., 2011). Moreover, the tsunami was observed to enter Kuji Bay in the form of a non-breaking bore and to evolve into a breaking bore as it propagated into shallower waters. Inside the harbor, after overtopping the offshore seawalls, the tsunami waves became an undulating breaking bore.

2.1 Tsunami-like bores

In general, tsunamis have been observed to reach coastal areas in the shape of bores: steep fronted waves followed by a semi-stable water flow. Different parameters have been proposed to classify the bores' magnitude. The most common parameter used in the literature to classify bores is the bore strength (Miller, 1968 and Yeh et al., 1989), represented by its Froude number:

$$F = \frac{U_b - u_0}{c_0} \tag{1}$$

where U_b is the speed of the bore propagation, u_0 is the velocity of the flow in front of the bore, $c_0 = \sqrt{g h_0}$ is the celerity, g is the acceleration due to gravity and h_0 is the still water depth in front of the bore. Based on physical experiments, bores are classified as undulating for $F < 1.25$, undulating-breaking bores for $1.25 < F < 1.5$, and breaking bores for $F > 1.55$ (Miller, 1968).

Based on the observations of tsunamis reaching coastal areas, the analysis of the 2011 tsunami video reaching Kuji bay (Nakagi et al., 2016), and results of numerical model studies from both events (Li, 2017; Takahashi and Tomita, 2013), it is reasonable to conclude that tsunamis reach coastal areas in the form of long bores with a strength range $1.18 < F < 1.745$ at 10m water depth. To simulate realistic tsunamis, the target of this study is to simulate the longest bores the physical set-up allows with a strength range $1 < F < 2$ and water depths h_0=0.1 m and 0.2 m (scales 1:100 and 1:50, respectively).

3 Bore generation theory

Based on the non-linear shallow water equations (NLSWEs hereafter), Stoker (1957) derived the conditions of a bore with height (h_b) and fluid velocity behind the bore (u_b) moving into waters with depth (h_0) and fluid velocity (u_0), lower than the incoming fluid velocity. From these conditions, Stoker (1957) and Liggett (1994) derived the relations between the bore strength (Eq. 1) and the bore characteristics:

$$\frac{u_b}{c_0} = F\frac{\sqrt{1+8F^2}-3}{\sqrt{1+8F^2}-1} \tag{2}$$

$$\frac{h_b}{h_0} = \left(\frac{c_b}{c_0}\right)^2 = \frac{1}{2}\left(\sqrt{1+8F^2}-1\right) \tag{3}$$

One of the simplest ways to generate a bore is to move a wall with constant velocity, pushing still water, as shown in Stoker (1957). This movement will generate a shock wave that will propagate with speed U_b. In this case, the fluid velocity behind the bore (u_b) will be equal to the paddle velocity (u_w).

The bore generation using a DB system can be formulated using the method of characteristics:

$$\frac{u_b}{c_0} + 2\frac{c_b}{c_0} = \frac{c_1}{c_0} \tag{4}$$

where c_1 is the wave celerity on the upstream side of the gate and c_0 is the wave celerity on the downstream side (Fig. 1). Substituting eq. (2) and eq. (3) into eq. (4), the bore strength can be calculated as function of the initial water depths ratio on both sides of the gate, and vice-versa.

4 Bore swash flows theory

The NLSWEs have also been used to study the swash flows produced by bores on a plane beach. Whitham (1958) derived his formula for the evolution of a bore on a plane slope. Later, Keller et al. (1960) provided a solution for Whitham's formula, predicting that bores will collapse as they reach

the shoreline, and that the water velocity behind the bore (u_b) and the bore front velocity (U_b) will approach a common value U_s at the shoreline. In their work, they identify a relationship between this velocity limit and a constant of integration, A, of the form:

$$U_s = 1.763\sqrt{gA} \tag{5}$$

where the constant of integration A can be determined using Keller et al. (1960) solution at a point in which the bore strength and the water depth are known (e.g. at the toe of the slope). In addition, Shen and Meyer (1963) derived the motion of the shoreline generated by the bore collapse:

$$x_s(t) = U_s t - \frac{1}{2} g s t^2 \tag{6}$$

where x_s is the shoreline position, u_s is the shoreline velocity, s is the beach slope (s=tanθ) and t=0s corresponds to the bore collapse time. It can be seen that the parabolic motion is driven only by gravity, and the maximum run-up distance (X_s) and run-up height (R) can be calculated as:

$$X_s = \frac{{U_s}^2}{2gs} \tag{7}$$

$$R = \frac{{U_s}^2}{2g} \tag{8}$$

Stoker (1957) also describes the reflection of a bore from a rigid vertical wall. For this case, the incoming bore flows towards a body of water at rest generating a hydraulic jump, which propagates upstream. The reflected bore height (h_r) can be found by solving equation (2) and equation (3) for a given u_b, c_b and being $-1 < F < 0$.

5 Experimental set-up

The physical experiments have been carried out in the wave flume of the Hydraulic Laboratory at National University of Singapore (NUS). The flume is 36 m long, 0.9 m high and 0.9 m wide. A 5m long stroke WM is installed at one end of the flume, a DB system is placed at 17.6m from the WM zero position and a glass slope has been installed at 11.1 m from the DB gate (fig. 1).

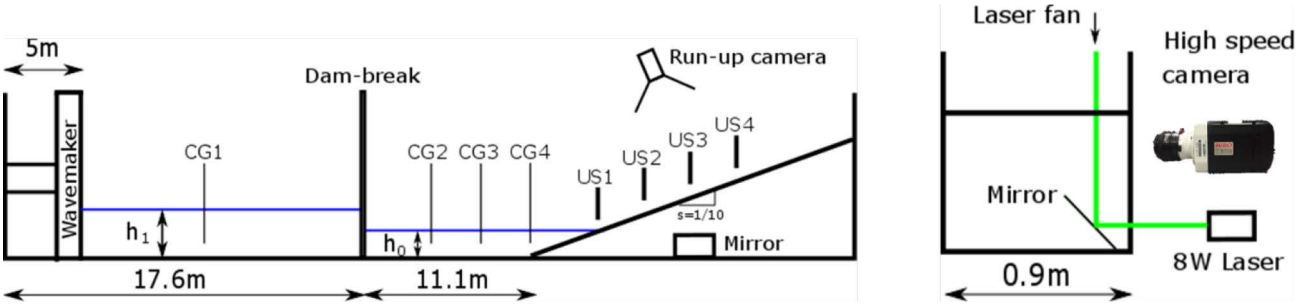

Fig. 1. Wave flume in the NUS Hydraulic Laboratory (not to scale) and experimental set-up.

The WM can reach velocities up to 2.5 m/s with a maximum 3.5 m/s^2 acceleration. It is driven by two parallel linear actuators controlled by an AC Servo Motor. A flexible rubber seal has been installed at the paddle sides and bottom to minimize water leaks. In addition, two reed switches have been installed at the paddle for triggering purposes.

Using a pneumatic system the DB has been designed to fully open the gate (0.9m) in less than one second. The gate has no railing on the flume walls or flume bottom, and it has been sealed with a customized rubber seal that covers the gate sides and bottom. Two reed switches have been installed in the system to know if the gate is open or closed, allowing synchronization between the gate, the sensors and other systems installed in the flume. The gate movement can be triggered manually or by using a trigger signal.

The wave flume is equipped with four capacitance gauges (CG) and four ultrasonic sensors (US). All the sensors are connected to a DAQ system to ensure a synchronized data acquisition. A video camera has been installed on top of the flume over the slope area to film the bores run-up. A HSPIV (High Speed Particle Image Velocimetry) system measures the flow velocities in a 2D plane during the surf and swash flows. The system's camera is capable of filming at 800 fps at maximum resolution

(2560x1600) and the lens selected provides a high image quality and negligible image distortion. An 8 W 532 nm continuous laser, equipped with an optical sheet unit, is being used as the light source to illuminate the particles in the water. For the water seeding, hollow-glass spheres have been used. A mirror has been placed below the glass slope with a 45°angle to the bottom so it reflects the horizontal laser fan perpendicular to the slope at 153.7 mm parallel to the flume wall (fig. 1), where the laser-fan is 2mm wide. The fluid velocities have been calculated using the free-license software PIVlab (Thielicke and Stamhuis, 2014). The set-up starts with an initial interrogation window of 128x128 px and has two passes until the last interrogation window of size 32x32 px. All the passes have a 50% overlapping step; giving a final resolution of 16x16px (i.e. 2x2 mm for the current setup).

6 Numerical model

Numerical simulations have been carried out and compared with the measured swash flows produced by an undulating bore in section 7.5. The numerical model used is olaFlow (Higuera 2018), a CFD model based on OpenFOAM that solves the Navier-Stokes equations with a moving free surface. The simulations presented in this study have been carried out in a mesh with 340k cells using the k-Ω SST turbulence model. The minimum grid height is 0.2 mm at the bottom boundary to capture the bottom boundary layer. The free surface readings from the first gauge are used as input to generate the undulating bore in the numerical computations, where the input velocities have been calculated using the linear shallow water theory.

7 Results

7.1 Wavemaker generated bores

To generate the longest bores, the WM paddle maximum displacement, 5 m, has been used in all the experiments. The WM has been configured to reach the target constant velocity for each case (u_w) with the maximum acceleration. Because strong bores generated with the WM start to decay before reaching the slope, bores stronger than $F = 2$ need to be generated to achieve the target strengths at the toe of the slope. Therefore, bores with input strength from $F = 1.05$ to $F = 3$ have been generated. In fig. 2 the mean dimensionless free surface elevations (FSE hereinafter) for three repetitions with plus-minus one standard deviation for bores with $F = 1.2$ and $F = 1.6$ are plotted.

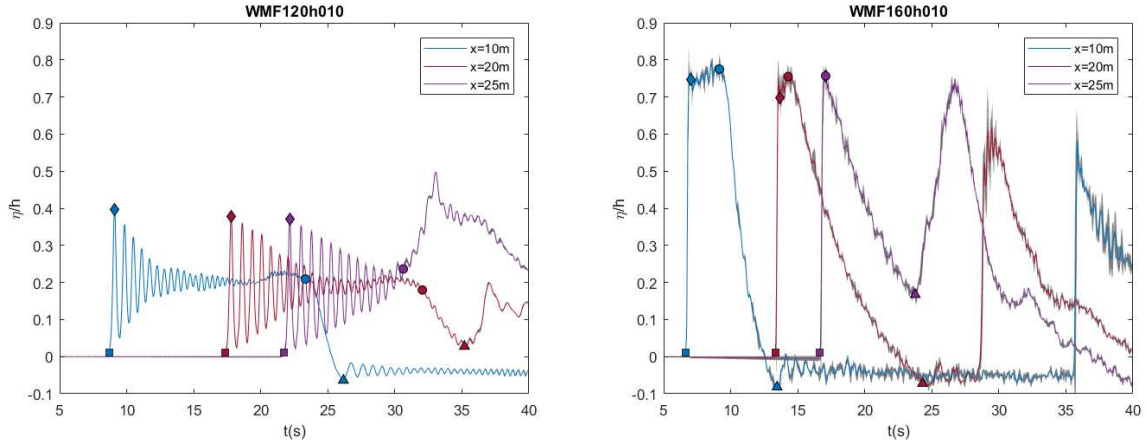

Fig. 2. Mean dimensionless FSE measured for WM generated bores with input strength F=1.2, on the left, and F=1.6, on the right, at CG1 (10 m) in blue, CG2 (20 m) in red and CG3 (25 m) in purple, plus-minus one standard deviation in grey (almost zero for WM generated bores). The x-axis zero (time) corresponds to the time the WM starts to move. Squares point the bore arrival times, diamonds point the bore plateau beginning, circles point the bore plateau end and reflected bore arrivals and triangles point the bore tail end.

As expected, the bores with input strength $F = 1.2$ have an undulating bore front and the bores generated with input strength $F = 1.6$ are breaking bores without undulations. The lack of grey areas in fig. 2 points out that the repeatability for WM generated bores is very good. For the non-breaking case the grey areas are imperceptible. For the breaking case, grey areas can be observed in the plateau

and tail, but these are still small. The results also show that bores generated with smaller input strengths have longer periods than the bores generated with larger strengths. For bores with input strength F = 1.2 the reflected bore from the slope reaches CG3 even before the plateau ends. In addition, bore periods also decrease as the bores propagate. For the case of F = 1.6, at CG3, the plateau front and end meet at the same point, becoming a decaying bore. Stronger bores start to decay earlier, losing strength as they propagate.

7.2 Dam-break generated bores

The DB system has been configured to fully open in less than one second, releasing the water from the 17.6m long reservoir. In fig. 3 the mean dimensionless wave heights with respect to the downstream water depth (h_0), plus-minus one standard deviation, for three DB generated bores with F = 1.2 and F = 1.6 have been plotted. Similar to WM generated bores, the bore front for the case of F = 1.2 shows undulations without breaking in the constant water depth region, and bores with strength F = 1.6 show a steep breaking front followed by smaller undulations.

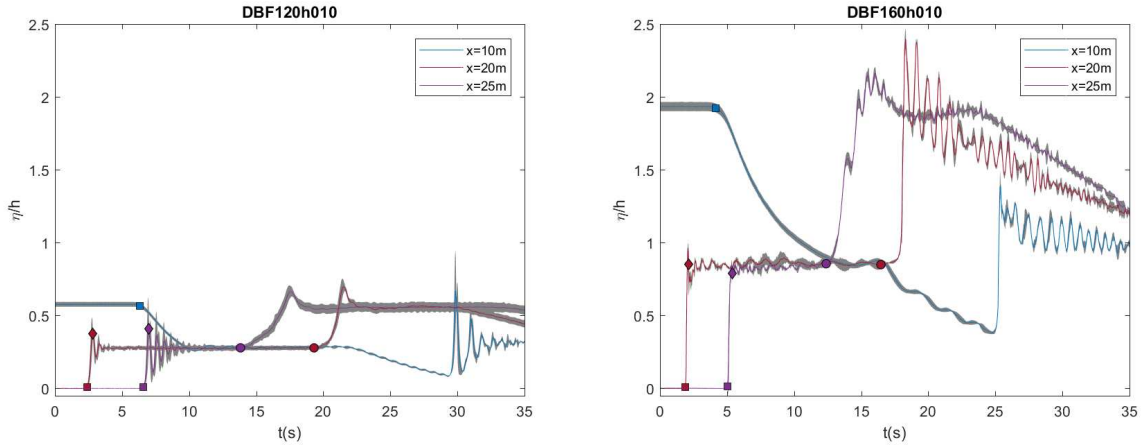

Fig. 3. Mean dimensionless FSE measured for DB generated bores with input strength F=1.2, on the left, and strength F=1.6, on the right, at CG1 (10 m) in blue, CG2 (20 m) in red and CG3 (25 m) in purple, plus-minus one standard deviation in grey. The x-axis zero (time) corresponds to the time the DB gate starts to open. Squares point the depression arrival for CG1 and the bore arrivals for CG2 and CG3, diamonds point the bore plateau beginning, circles point reflected bore arrival times.

The greyed areas show that the repeatability of DB bore generation system is good, but not as good as the WM system. At CG1 (within the reservoir) the experiments show slightly different upstream and downstream water depth ratios. This is because of the difficulty in setting up the exact same water depths for each experiment in a flume of this size. Therefore, it is not surprising to see some variance in the measured bore heights. For the non-breaking case, larger deviations are observed in the bore front, compared to other cases. Another challenge is maximizing the repeatability is in controlling the gate opening time. The mean gate opening time measured for all the DB cases is 0.871 s, with a standard deviation of 0.078 s. Because the time when the gate starts to open has been chosen as the reference zero time for the experiments, variations in the gate opening will generate small differences in the bore arrival times. These arrival time differences are more obvious in the non-breaking case because they generate a phase difference in the bore front undulations, which is not present on the breaking bores.

The DB generated bores have shown to be longer than WM generated bores for strengths F >1.15. For smaller strengths it is difficult to assess the bore length as the reflections catch-up with the gauges before the bore tail arrives. In addition, DB generated bores keep these large lengths even for the strongest cases. On the other hand, the DB generated bores repeatability is not as good as the WM generated bores, and this is crucial when carrying out PIV analysis.

7.3 Bores measurements at the slope

In this section, the measurements of the capacitance gauge at the toe (CG4) and the non-intrusive ultrasonic sensor located above the initial shoreline are used to analyze the swash flows of WM and

DB generated bores on the smooth 1:10 slope. The incoming bore strengths have been measured at the constant water depth section from the time arrivals between CG3 (x = 25 m) and CG4 (x = 28.7 m). The inundation water depth values have been defined as the maximum height measured at the initial shoreline section.

The dimensionless FSE measured at the toe of the slope and at the initial shoreline location are shown in fig. 4. For the F = 1.2 case, the waves were non-breaking at the toe but broke during the swash. The bores with input strength F =1.6 were already breaking at the toe and collapsed during the swash. It can be observed that the ultrasonic sensors cannot provide continuous readings for very steep free surface (undulations for the F = 1.2 case and front of the bore for the F = 1.6 case). The measurements at the toe of the slope show the outstanding repeatability for WM generated cases (the grey area representing the standard deviation is almost non-existent for the non-breaking case, and very small for the breaking case), and the ensemble of the ultrasonic sensor measurements provide an accurate representation of the wave heights at the shoreline.

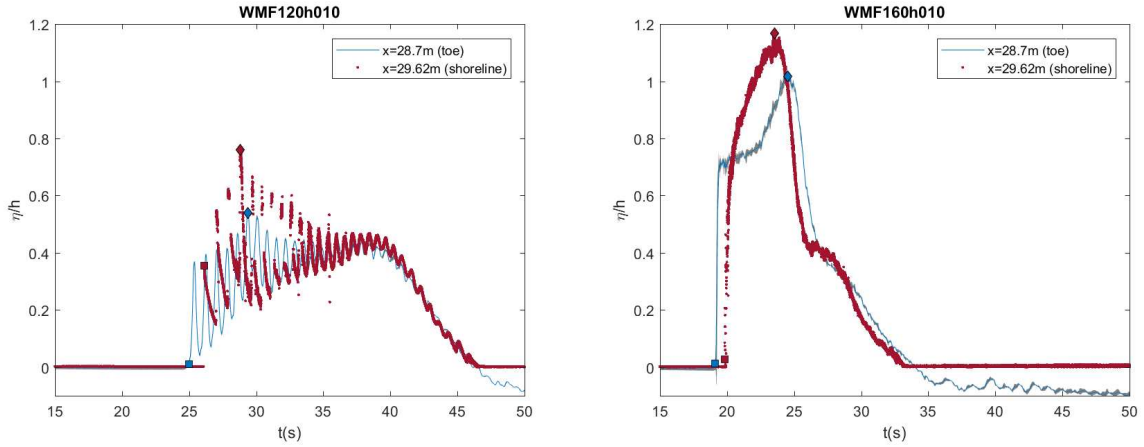

Fig. 4. Mean dimensionless FSE measured for 3 WM generated bores with input strength F=1.2, on the left, and F=1.6, on the right, at the slope toe (CG4 at 28.7 m) in continuous blue line, plus-minus one standard deviation of the measurements in grey, and the ensemble of 3 repetitions at the initial shoreline location (US at 29.62 m) in red dots. The x-axis zero (time) corresponds to the time the WM starts to move. Squares point the bore arrival times and diamonds point the maximum heights measured.

It is difficult to differentiate between the incoming and reflected bore at the toe and the shoreline for both cases. The undulating bore was observed to be longer than the breaking case in the constant water depth section, and therefore it is not surprising that the swash flow also has a longer period. In the undulating case, the undulations height increase until they reach its maximum at the 6th undulation at the toe and at the 4th undulation at the shoreline. Next, the undulations amplitude start to decrease and the crests and troughs converge towards a semi-stable water level height, for both gauges, before the water level starts to decrease simultaneously at both gauges. On the other hand, the water depths for the breaking case start to decrease right after the maximum level is reached, without any sign of an inundation plateau. This is not surprising as the bores for this case were observed to be already decaying at CG3, 3m before the toe. The maximum water height is reached at the shoreline before the toe, indicating this maximum is most probably reached during the bore reflection.

The water depths at the toe and the shoreline for the DB generated bores with input strength of F = 1.2 and F = 1.6 are shown in fig. 5. Like the WM generated bores, the bores with strength F = 1.2 show non-breaking undulations at the toe and break during the swash. For the stronger case, F = 1.6, the bores reach the toe of the slope as breaking walls of water and collapse during the swash flows into tongues of water propagating up the slope. The CG measurements deviation at the toe, in grey, and the ultrasonic sensors' measurements variability at the shoreline show that the DB generated bores repeatability is not as good as the WM generated bores, as observed in the previous section. The DB generated bores with strength F = 1.2 have similar fronts but produce larger inundation depths than the respective WM generated bores. In addition, the inundation plateau is much larger and with a more stable height than the observed during the WM experiments. For the stronger case, the front from the DB bores differ from the WM generated bores. Right after the bore arrival the water depth increases fast and constantly until it reaches its maximum depth, almost double than the maximum depth measured for the WM cases. In addition, the front is followed by a semi-stable inundation plateau that

was not observed for the WM shorter bores. Finally, the inundation plateau for the stronger bore is shorter than the plateau from the undulating case.

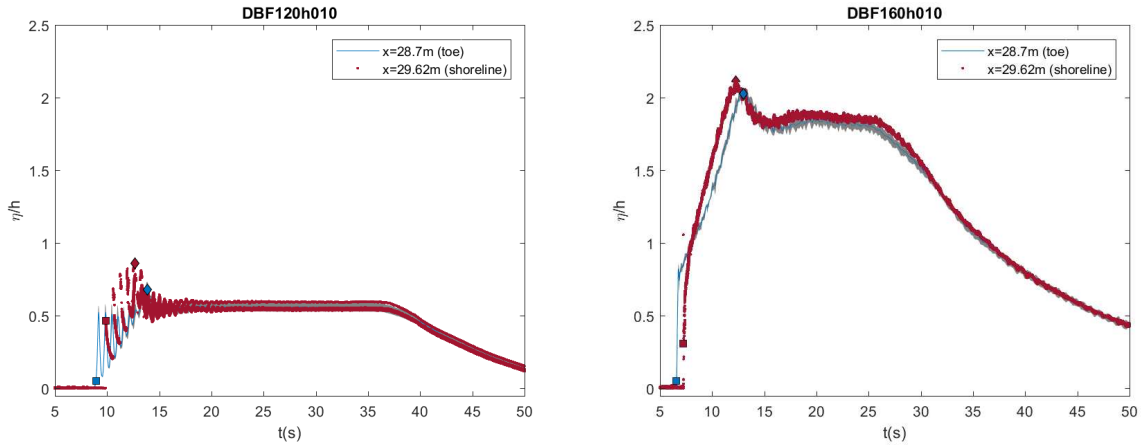

Fig. 5. Mean dimensionless FSE measured for 3 DB system generated bores with input strength F = 1.2, on the left, and F = 1.6, on the right, at the slope toe (CG4 at 28.7 m) in continuous blue line, plus-minus one standard deviation of the measurements in grey, and the ensemble of 3 repetitions at the initial shoreline location (US at 29.62 m) in red dots. The x-axis zero (time) corresponds to the time the DB starts to move. Squares point the bore arrival times and diamonds point the maximum heights measured.

7.4 Inundation depths and run-up measurements

The maximum inundation water depths at the shoreline and maximum run-up values have been measured for a series of bores with strengths $1 < F < 2$ for two different initial water depths: h_0 = 0.1 m and h_0 = 0.2m. The bores strength have been measured from the arrival times between CG3 and CG4. The inundation depths have been measured as the maximum height registered by the ultrasonic sensors installed at the initial shoreline, and the maximum run-up values have been captured using the camera installed above the slope. The inundation water depths at the shoreline and the run-up measurements have been plotted in fig. 6. The inundation depths are compared with the calculated heights of the reflected bores on a vertical wall for the given incoming bore strengths. The run-up measurements are compared to Shen & Meyer (1963) analytical solution (section 4) and to Miller (1968) experimental results (s=1:11.43).

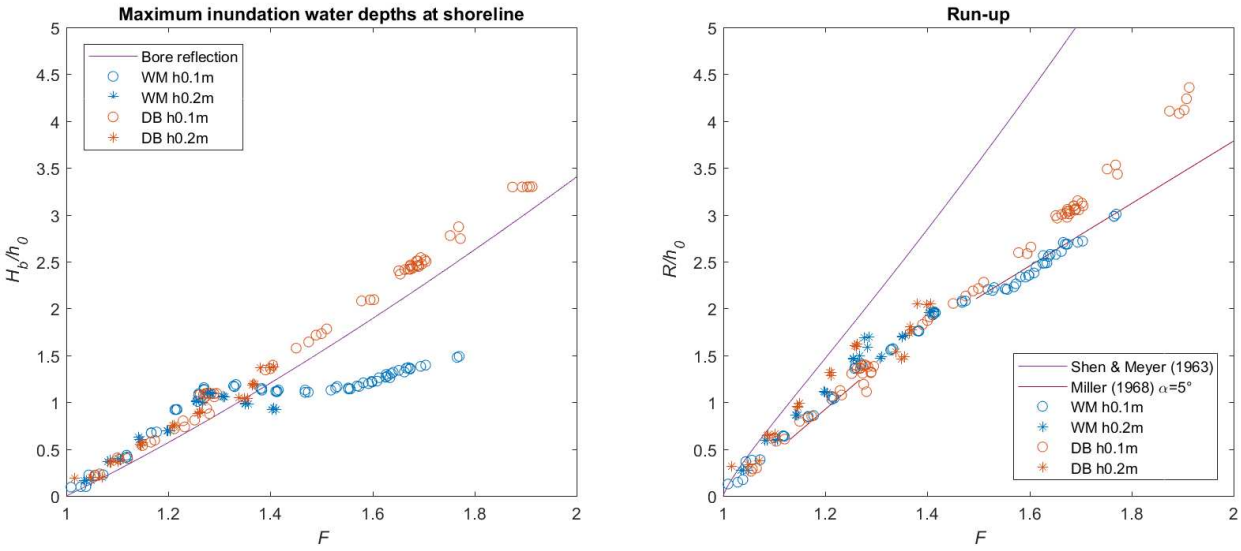

Fig. 6. Dimensionless maximum water depths at the shoreline (left) and dimensionless maximum run-up (right) to bore strengths measured between CG3 and CG4. WM cases in blue and DB cases in orange. Circles: h_0 = 0.1 m. Stars: h_0 = 0.2 m. Inundation water depths: the purple line represents the height of a bore reflected on a vertical wall, the run-up purple line corresponds to Shen & Meyer (1963) analytical solution and red line to Miller (1968) results.

The inundation depth results show good agreement for bores generated with both systems and for both water depths for the weaker bores ($F < 1.3$). For stronger bores, the WM generated bores inundation depths decrease, compared to the DB system bores. The reduction is larger for the larger initial water depth ($h_0 = 0.2$ m). The DB generated bores keep a trend slightly above the bore reflection heights. In the run-up measurements a similar trend can be observed, where the WM bores run-up values start to deviate from the DB bores for a larger strength ($F > 1.5$). After this drop, the run-up values keep a similar slope to Miller (1968) results. However, Miller results start to deviate from the initial trend earlier, for $F = 1.25$. A similar deviation can be observed for WM bores with $F > 1.5$. The run-up generated by all WM and DB bores are smaller than the predicted by Shen & Meyer (1963) solution.

The results point out that the bore period/length plays an important role in the swash flows. It seems that a minimum bore length at the slope toe is required to achieve the maximum inundation depth and run-up, and that the minimum required length to achieve the maximum inundation depth is larger than the one required for the maximum run-up. This is to be expected because to achieve the maximum run-up, the bore only needs to be long enough to reach the shoreline without decaying, whereas the maximum inundation depths are reached during the bore reflection. Short bores will become decaying bores during the climbing of the slope (pointing probably to the initial separation from the original trend), and bores that arrive as decaying bores will continue to decay, generating smaller run-up values (presumably the parallel but smaller run-up values observed for WM bores with strength $F > 1.55$). The fact that the WM inundation depths start to decrease earlier for the initial water depth $h_0 = 0.2$m agrees with the idea of a required minimum length, as WM generated bores for larger water depths are relatively shorter compared to the bores generated in shallower waters for the current generation set-up. The length of the bores was not analyzed in Miller (1968) and Yeh et al. (1989), who observed similar features in the run-up and velocity measurements. They attributed the smaller results to the transition between undulating and breaking bores and to the slope roughness and inclination. If the reason for Miller's under predicted run-up results is related to the short lengths of the study's bores, as the evidence in this study suggest, Miller's results would also imply that milder slopes require longer bores in order to achieve the maximum run-up. Nevertheless, the influence of the bore length does not discard the influence of the slope roughness, as shown by Miller (1968). The small difference between the bores maximum run-up for strong DB cases could be result of the slope roughness, which is expected to have a larger influence on bores propagating for longer distances on the slope.

Finally, it can be observed in fig. 5 that the maximum inundation is produced during the initial reflection, which is slightly larger than the plateau height. This agrees with the DB bores inundation results compared to the analytical bore height reflection on a vertical wall, which represent the depth of the inundation plateau.

7.5 High Speed Particle Image Velocimetry (HSPIV) and Numerical results comparison

The PIV system has been set-up with an interrogation window parallel to the slope at the shoreline region. The case analyzed is a WM generated bore with initial water depth $h_0 = 0.24$ m and input strength $F = 1.105$. The experiments have been recorded at 500 fps for time windows of 2052 frames (due to memory limitations). Repetitions over seven time windows with 0.6 s overlap have been necessary to record the whole swash event. Ten repetitions have been carried out for each time window, i.e. the case has been repeated 70 times for the PIV analysis.

The left panel in fig. 7 shows the FSE measured at 0.107 m above the initial shoreline on the slope direction by an ultrasonic sensor for 8 repetitions, the mean FSE plus-minus one standard deviation measured using the PIV system and the calculated FSE from the numerical computations. On the right panel, the depth-averaged velocities on the slope direction plus-minus one standard deviation calculated from the PIV results at the same location and the calculated depth-averaged velocities from the numerical computations have been plotted.

The measurements from the ultrasonic sensor, recorded before the PIV system was installed, have been used to verify the PIV free surface interpolation process. Both results superimpose almost perfectly, indicating the PIV free surface detection process is accurate. The numerical model results heights match very close the experimental measurements, especially during the first 5 waves. However, it can be observed that the numerical FSE is slightly lower during the plateau inundation. The numerical results of velocity are also very close to the PIV measurements, except for some disturbance when the FSE values are close to zero (before and after the bore) and for the peak

velocities at the bore arrival, which are 1.34 m/s and 2.34 m/s for PIV measurements and the numerical result respectively. These differences are almost negligible when the velocities are multiplied by the wave height to calculate the bores' discharge.

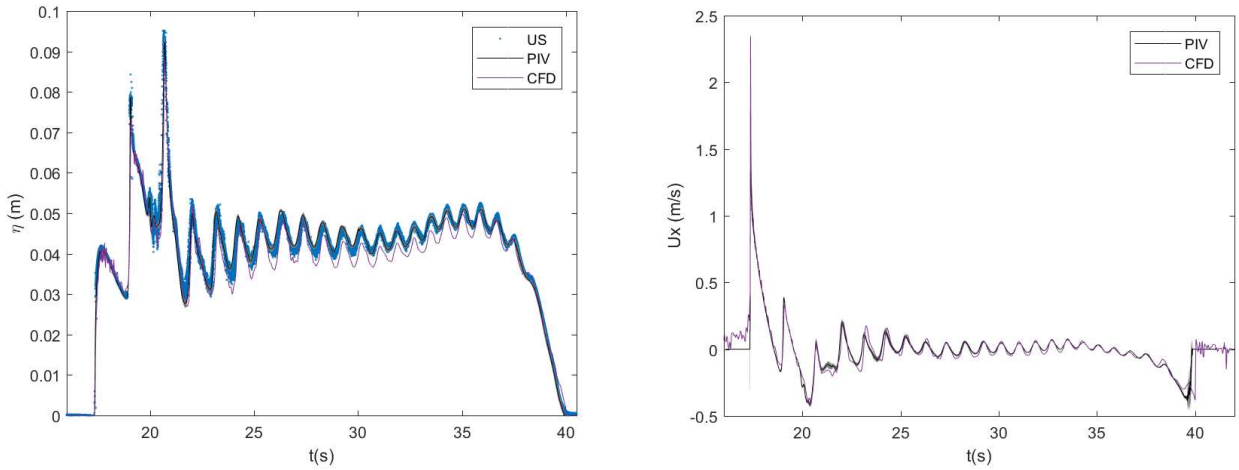

Fig. 7. Free surface measured at 0.107 m above the initial shoreline on the slope direction, on the left panel, and depth-averaged velocities in the slope direction at the same location, on the right panel. Blue dots represent measurements from the US for 8 repetitions. The continuous black lines and greyed areas represent the PIV mean measurements plus-minus one standard deviation respectively. In purple, CFD results.

The results show how the undulating bore has three initial larger waves and is then followed by a semi-stable plateau inundation depth. The maximum height is reached during the third wave, but the velocity measurements show that this wave is produced by the reflection, as the velocities before and after are negative. The maximum velocities are reached during the first wave, and are close to zero during the inundation plateau. Finally, the velocities become negative during the bore run-down.

8 Conclusions and future work

In this study we have used a wavemaker and a dam-break to generate tsunami-like bores with different lengths and strengths in the laboratory. Using measurements from capacitance and ultrasonic gauges and from a HSPIV system, we have analyzed the bores' shape and evolution during their propagation over a horizontal flume and during run-up over a smooth glass beach of 1:10 slope.

The repeatability of the wavemaker generated bores is outstanding, however, the results also show that the bores generated using this system are not long enough to investigate the complete flooding process for the strongest bore cases. On the other hand, even if the repeatability of the dam-break generated bore is not as good, this system can generate very long bores capable of sustaining semi-stable inundations for tens of seconds. For non-decaying bores, both wavemaker and dam-break generated bores show similar characteristics and results, indicating both systems are capable of generating uniform bores comparable among themselves. The PIV results show good agreement with the sensors in the flume and with the numerical results both for water depths and flow velocities.

The results presented show the significance of the bore lengths and the importance of their analysis in bore classification. We propose to classify bores as long bores when their plateaus are long enough to generate the complete swash, i.e., reach the run-up and inundation depths for a given slope similar to the run-up and inundation depths an infinite uniform bore would generate.

In the context of tsunamis reaching coastal areas, the results point out that transient long waves flooding process can be divided in three stages. First, the fast propagating bore front reaches dry areas followed by a flow with large velocities. As the flow velocities decrease due to the bore reflection, the water depths increase until they reach a semi-stable inundation depth, similar to the height the bore reflection on a vertical wall would produce. Next, the semi-stable inundation is kept for a period that will depend on the bore length. If a second wave were to arrive to the coast during this inundation period, the wave will probably flood larger areas than the initial wave due to the higher initial shoreline position. Finally, the wave retreats with flow velocities that will depend on the tsunami wave tail.

An extended PIV dataset for cases with different strengths and with measurements at different locations is necessary for further validation of the numerical model. Next, numerical simulations of transient long waves-bores are essential to study the minimum lengths required to generate the complete flooding processes produced by very long waves. These minimum lengths can then be used as a criteria to classify long waves generated in laboratories as tsunami waves.

Acknowledgements

The authors would like to acknowledge the support from the National University of Singapore (NUS) and the Earth Observatory of Singapore (EOS). I. Barranco would like to thank NUS for the PhD Scholarship support.

References

Goseberg, N., Wurpts, A., and Schlurmann, T., 2013. Laboratory-scale generation of tsunami and long waves. Coastal Engineering, 79:57 – 74.

Higuera, P., 2018, olaFlow [Software]. http://doi.org/10.5281/zenodo.1297013

Imamura, F., Goto, K., and Ohkubo, S., 2008. A numerical model for the transport of a boulder by tsunami. Journal of Geophysical Research: Oceans, 113(C1):n/a–n/a. C01008.

Keller, H. B., Levine, D. A., and Whitham, G. B., 1960. Motion of a bore over a sloping beach. Journal of Fluid Mechanics, 7(2):302–316.

Li, L., 2017, A review of the 2004 Sumatra-Andaman Earthquake source model, Annual report.

Liggett, J., 1994. Fluid mechanics. McGraw-Hill.

Liu, P. L. F., Cho, Y.-S., Briggs, M. J., Kanoglu, U., and Synolakis, C. E., 1995. Runup of solitary waves on a circular island. Journal of Fluid Mechanics, 302:259–285.

Miller, R. L., 1968. Experimental determination of run-up of undular and fully developed bores. Journal of Geophysical Research, 73(14):4497–4510.

Mori, N., Takahashi, T., Yasuda, T., and Yanagisawa, H., 2011. Survey of 2011 tohoku earthquake tsunami inundation and run-up. Geophysical Research Letters, 38(7).

Nakagi, T., Kosa, K., and Sato, T., 2016. Evaluation of properties of tsunami in kuji port. Journal of Japan Society of Civil Engineers, Ser. B2 (Coastal Engineering), 72(2).

Rossetto, T., Allsop, W., Charvet, I., and Robinson, D. I., 2011. Physical modelling of tsunami using a new pneumatic wave generator. Coastal Engineering, 58(6):517 – 527.

Schimmels, S., Sriram, V., and Didenkulova, I., 2016. Tsunami generation in a large scale experimental facility. Coastal Engineering, 110:32 – 41.

Shen, M. C. and Meyer, R. E., 1963. Climb of a bore on a beach part 3. run-up. Journal of Fluid Mechanics, 16(1):113–125.

Stoker, J. J., 1957. Water Waves, The Mathematical Theory with Application. Interscience Publishers, Inc.

Synolakis, C. E., 1987. The runup of solitary waves. Journal of Fluid Mechanics, 185:523–545.

Takahashi, K., and Tomita, T., 2013. Simulation of the 2011 tohoku tsunami in kuji bay using three-dimensional non-hydrostatic numerical model, Journal of Japan Society of Civil Engineers, Ser. B2 (Coastal Engineering) 69, 166-170.

Thielicke, W., Stamhuis, E. J., 2014. Pivlab-towards user-friendly, affordable and accurate digital particle image velocimetry in matlab, Journal of Open Research Software 2.

Whitham, G. B., 1958. On the propagation of shock waves through regions of non-uniform area or flow. Journal of Fluid Mechanics, 4(4):337–360.

Yeh, H. H., Ghazali, A., and Marton, I., 1989. Experimental study of bore run-up. Journal of Fluid Mechanics, 206:563–578.